



In vitro model systems for studying the impact of organic chemicals on the skin barrier lipids

Daniël Groen^a, Fabienne Berthaud^a, Joke A. Bouwstra^b, Christian Chapuis^a, Gert S. Gooris^b, Mila Boncheva^{a,*}

^a Corporate R&D Division, Firmenich SA, Geneva, Switzerland

^b Leiden/Amsterdam Center for Drug Research, Department of Drug Delivery Technology, Leiden, The Netherlands

ARTICLE INFO

Article history:

Received 23 May 2013

Received in revised form 26 September 2013

Accepted 3 October 2013

Available online 12 October 2013

Keywords:

Stratum corneum

Molecular organization

Skin barrier lipids

Infrared spectroscopy

X-ray diffraction

ABSTRACT

This paper describes two synthetic lipid models designed to replace human stratum corneum (SC) in studies of the impact of volatile organic chemicals on the molecular organization of the skin barrier lipids. The models built upon previously developed self-assembled lipid membranes which have composition and 3D organization similar to those of the lipid matrix in SC. In one model the target chemicals were incorporated in the lipids before their self-assembly, and in the other one they were applied on top of a preformed lipid membrane. The chemicals could be incorporated within the model membranes in quantities close to those reached within human SC upon heavy surface loading. The dose-dependent effects of the chemicals on the lateral molecular organization in the models were qualitatively identical to those observed by infrared spectroscopy in human SC. The models facilitated the interpretation of X-ray diffraction profiles used to determine the nature of the interactions between the chemicals and the lipid lamellae and the position of the exogenous molecules within the unit cell of the lipid phases. These model systems are suitable for *in vitro* studies in the areas of skin biophysics, dermatology, transdermal drug delivery, and risk assessment.

© 2013 Elsevier B.V. All rights reserved.

1. Introduction

The lack of a reliable experimental strategy—one combining an appropriate substrate and sound methodology—can be a serious bottleneck in evaluating the impact of exogenous chemicals on the biophysical and physicochemical properties of the human skin barrier. Such investigations are essential for the successful design of safe topical products (e.g., cosmetics, transdermal drugs, and insect repellents) and for understanding—and thereby, finding ways to counteract—the damages caused by hazardous chemicals, environmental pollutants, and chemical warfare agents to the topmost skin layers. Here, we demonstrate the use of synthetic lipid membranes to investigate the influence of volatile organic compounds on the molecular organization of the skin barrier lipids. The impact of the chemicals on the lateral packing and conformational order of the lipid chains in the synthetic membranes observed by Fourier transform infrared spectroscopy

(FTIR) was qualitatively identical to the one observed in native human stratum corneum (SC). Small-angle X-ray diffraction (SAXD) studies showed that the chemicals can swell the lamellar lipid phases and pointed to their localization within the lipid lamellae.

The molecular organization of the extracellular lipids in the topmost skin layer, SC, is crucial for maintaining an efficient barrier to the evaporation of water from the viable skin tissues and to the skin penetration of exogenous molecules [1–7]. Most of the experimental evidence collected so far indicates that these lipids—comprising mainly ceramides, free fatty acids, and cholesterol in approximately equimolar proportions [8–10]—are arranged in extended lamellar sheets with two characteristic periodicities: one of around 13 nm (denoted as long periodicity phase, LPP) and one of around 6 nm (denoted as short periodicity phase, SPP) [11–14]. The lateral packing of the hydrocarbon lipid chains in these lamellae is predominantly orthorhombic (OR), with a small fraction of the lipids forming hexagonal (HEX) and liquid-crystalline (LIQ) phases [15–18]. The presence of lamellar structures of appropriate periodicity and containing high relative fractions of OR-packed lipids is essential for the low permeability of SC [19–21]. Chemicals that come into contact with the skin and are capable of admixing with the native SC lipids can, in principle, modify their molecular organization and, thereby, alter the permeability of the SC. Reliable measurement and quantification of these effects is essential for understanding skin homeostasis.

The combination of FTIR and SAXD is ideally suited to investigate the lateral and the lamellar organization in structured lipid ensembles [11]. Its application to study the effects of topically applied chemicals on SC

Abbreviations: ATR, attenuated total reflection; CC, diethyl 1,4-cyclohexanedicarboxylate; DA, dodecyl acetate; dFRM, perdeuterated fragrance raw material; EdT, Eau de Toilette; FRM, fragrance raw material; FTIR, Fourier transform infrared; FWHM_{scis}, full width at half height of the CH₂ scissoring band; GC/FID, gas chromatography with flame ionization detector; HEX, hexagonal; LIQ, liquid-crystalline; LPP, long periodicity phase; OR, orthorhombic; PBS, phosphate buffer saline; SAXD, small-angle X-ray diffraction; SC, stratum corneum; SCS, stratum corneum substitute; SPP, short periodicity phase; UL, γ -undecalactone

* Corresponding author at: Corporate R&D Division, Firmenich SA, P.O. Box 239, Route des Jeunes 1, CH-1211 Geneva 8, Switzerland. Tel.: +41 22 780 3027; fax: +41 22 780 3334.

E-mail address: mila.boncheva@firmenich.com (M. Boncheva).

lipids, however, is complicated by considerations regarding the choice of an appropriate substrate. Excised human skin is not readily available in sufficient quantities and is prone to considerable inter- and intra-individual variability in the molecular organization of the SC lipids [22–24]. Its replacement by animal (e.g., porcine) skin in studies of the SC lipid biophysics is not possible because of significant inter-species differences [17,25]. Finally, the interpretation of FTIR spectra collected from SC is not always straightforward because of the overlap of spectroscopic signals originating from the SC proteins and lipids [16,26].

The stratum corneum substitute (SCS) is a previously developed synthetic model of the SC extracellular lipids [27]. Its composition, although simplified, comprises the main lipid classes and relevant subclasses found in the SC lipid matrix, and its 3D molecular organization is similar to the one of the SC lipids [28]. The preparation of the model is simple and fast; it consists in mixing the synthetic lipids in the desired proportions, depositing the mixture on an appropriate substrate, equilibrating it at elevated temperature, and letting the lipids self-assemble while slowly cooling down the sample [29]. Because of its similarity to the SC lipid matrix structure, reproducible preparation, and the possibility to control precisely its composition, the SCS has emerged as a suitable alternative for human skin in ranking the skin permeation of topically applied chemicals [30] and in studying the molecular organization of healthy, diseased, and treated SC [31–33].

In this work, we examined the suitability of the SCS as a surrogate for human SC in studying the interactions between SC lipids and volatile, lipophilic, organic molecules, a class of chemicals that frequently contact the skin due to their broad use as fragrance raw materials (FRMs), solvents, drug penetration enhancers, and cosmeceuticals. As model compounds we used three FRMs— γ -undecalactone (UL), dodecyl acetate (DA), and diethyl 1,4-cyclohexanedicarboxylate (CC)—chosen to have different combinations of lipophilicity (as measured by their log P values) and chemical functionality, and a medium volatility. We formulated two model systems based on the SCS which differed in their preparation: in one (denoted as mixSCS), the FRMs were admixed with the synthetic lipids before their self-assembly; in the other (denoted as topSCS), the FRMs were applied topically to the surface of a preformed SCS. To evaluate if the two models reproduce correctly the impact of the chemicals on the lipid organization in human SC, as a reference we used excised human skin treated topically with the same FRMs.

First, we examined the FRM content that could be reached in the two SCS models and in the SC of excised skin. At the end of the application period, we removed the surface excesses of FRMs and quantified the amounts of FRMs contained within the lipid lamellae by gas chromatographic analysis of dissolved topSCS and mixSCS samples and of 30 tape-strips applied to the excised skin samples. Next, we investigated the mixing of the FRMs with the synthetic and native SC lipids and their effect on the conformational order and the lateral organization within the lipid lamellae using FTIR spectroscopy. We collected transmission FTIR spectra from the mixSCS and topSCS samples and ATR-FTIR spectra at progressively greater depths within the SC during tape-stripping of the skin samples. To enable concurrent observation of the spectroscopic signals originating from the FRMs and the lipids, we used samples prepared as described above but treated with perdeuterated analogs of the FRMs (denoted as dFRM). Finally, we investigated the effects of the FRMs on the presence and the repeat distances of the LPP and the SPP, and the electron density distribution within the LPP in mixSCS and topSCS using SAXD.

2. Materials and methods

2.1. FRMs

UL, DA, and CC (Table 1) were supplied by Firmenich SA (Geneva, Switzerland), and their perdeuterated analogs (denoted as dUL, dDA, and dCC, respectively) were synthesized as described in Supplementary material.

2.2. Composition of the lipid and FRM–lipid mixtures

First, we prepared separate mixtures of ceramides and fatty acids. The ceramide mixture comprised (EOS)C30, (NS)C24, (NP)C24, and (NP)C16 (all from Cosmoform B.V., Delft, The Netherlands) in a molar ratio of 16:56:18:10; in these acronyms of the ceramide structure, N and EO denote the type of fatty acyl chain (non-hydroxy or ω -hydroxy ester-linked to a linoleic acid, respectively), S and P denote the type of sphingoid base (sphingosine or phytosphingosine, respectively, both containing 18 carbon atoms), and Cxx indicates the number of carbon atoms in the fatty acyl chain. The fatty acid mixture comprised palmitic, stearic, arachidic, behenic, tricosanoic, lignoceric, and cerotic acid from Sigma-Aldrich Chemie GmbH (Schnelldorf, Germany) in a molar ratio of 1.8:4.0:7.7:42.6:5.2:34.7:4.1. The proportions of the individual ceramides and fatty acids were selected to mimic as closely as possible those found in human SC with the available synthetic molecules [34–37]. Next, we combined appropriate amounts of the ceramide mixture, cholesterol (from Sigma-Aldrich Chemie GmbH, Schnelldorf, Germany), and the fatty acid mixture to result in an equimolar ratio of the three lipid classes, and transferred them to hexane:ethanol (2:1, v/v) with a total lipid concentration of 4.5 mg/mL. For preparation of mixSCS, we diluted the FRMs 10 times with hexane:ethanol (2:1, v/v) and added an appropriate volume of these solutions to the lipid solution to obtain FRM:lipid molar ratios of 1.67 and 3.33.


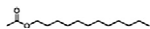
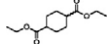
2.3. Preparation of SCS and mixSCS

We sprayed the lipid and FRM–lipid solutions on the substrates (CaF₂ windows from Specac, Kent, UK and Nuclepore polycarbonate filter disks with a pore size of 50 nm from Whatman, Kent, UK) using a Linomat IV (Camag, Muttenz, Switzerland; for details, see Supplementary material). After spraying, we placed the samples covered with a glass chamber on a hotplate and equilibrated them at $78 \pm 1^\circ\text{C}$ (temperature at the sample surface) for 10 min. (For SCS samples prepared for bench-top SAXD measurements, we used a slightly modified protocol: first, we equilibrated the SCS samples at $90 \pm 1^\circ\text{C}$ for 1 min, and then within 10 min reduced the temperature to $78 \pm 1^\circ\text{C}$.) Preliminary experiments showed that the mixSCS samples suffered considerable losses of FRMs during spraying and the high-temperature equilibration procedure (data not shown). To minimize these losses, we performed the equilibration step in a saturated FRM gas environment created by placing 25 μL of the corresponding FRMs in a vial inside the glass chamber. After the high-temperature equilibration, we let the self-assembly of the lipid lamellae proceed while slowly cooling down the samples to room temperature (approximately 30–50 min). After their preparation, we rinsed the surface of mixSCS samples with 0.6 mL ethanol to remove any FRMs that may have adsorbed to the surface during the equilibration in saturated FRM atmosphere (see also Section 2.5).

2.4. Treatment of excised skin and topSCS with FRMs

We used abdominal skin from Caucasian female subjects aged 45 to 53, dermatomed to a nominal thickness of $579 \pm 20 \mu\text{m}$ (Bioprédic Intl., Rennes, France), and stored at -20°C . Before use, we trimmed the skin to circles with a diameter of 20 mm, thawed each piece on absorbing paper, and cleaned the SC surface with three cotton swabs soaked with cold hexane, to remove traces of sebum. Before treatment, we placed a piece of skin (SC side up) on a static Franz diffusion cell filled with PBS buffer (150 mM, pH 7.4) containing 1% Tween-20 which was thermostated at 37°C , and let it equilibrate for 30 min. We delimited a test area of 0.95 cm^2 on top of the skin using a PTFE spacer with a circular hole ($d = 1.1 \text{ cm}$) in the middle. To treat the skin with the FRMs, we used dFRM formulated as simplified Eau de Toilette (EdT) solutions [30% (w/w) dFRM in ethanol:water (9:1, v/v)]. We applied 3 μL EdT on the skin surface using a 5- μL Hamilton syringe, and evenly spread the liquid over the test area; thus, the resulting dose delivered

Table 1
Fragrance raw materials (FRMs) used in this study.

Fragrance material	CAS no.	Structure	Molecular weight	log P	Vapor pressure [Pa]
γ -Undecalactone (UL)	000104-67-6		184.28	3.06	0.55
Dodecyl acetate (DA)	000112-66-3		228.37	5.78	1.61
Diethyl 1,4-cyclohexanedicarboxylate (CC) ^a	072903-27-6		228.28	3.09	1.68

^a The cis/trans ratio in protonated CC was equal to 80/20, and in perdeuterated CC—to 67/33.

to the skin surface was 780 μg dFRM/ cm^2 . Following the deposition of the FRMs, we let their interactions with SC proceed for 4 h. We performed all experiments using skin from three to five different donors.

We applied the FRMs to the surface of topSCS pure or formulated as model EdT solutions of concentrations varying between 6 and 50% (w/w) using either the Linomat instrument or the 5- μL -Hamilton syringe. Following the deposition of the FRMs, we let their interactions with the topSCS proceed for 6 or 16 h. At the end of this period, we rinsed the sample surface using the procedure employed with mixSCS. Using dFRM, we established that the volume of ethanol we used for the rinse is sufficient to remove any FRMs that may have remained at the sample surface at the end of the application period (data not shown).

2.5. Quantification of the FRM content in SC and SCS

Four hours after the application of EdT, we wiped the skin surface with three cotton swabs, to remove any FRMs remaining on the skin surface, and tape-stripped the SC 30 times using D-Squame tapes (CuDerm, Dallas, USA) as described elsewhere [38]. To quantify the amounts of FRMs within the SC, we extracted the 2nd to the 30th tapes (the first four pooled together, and the rest—in groups of five) by one-hour sonication in 1.5 mL iso-octane, and quantified the FRM concentrations in the extract by gas chromatography (GC/FID; for more details, see Supplementary material). As recommended in the regulatory guidelines [39], we did not take into account the FRM amounts found on the first tape since they might comprise also residual molecules from the SC surface. To establish the depth profiles of the FRM contents, we estimated the depth within SC reached by removing each tape-strip as previously described [40].

To account for the different lipid content within the SC and SCS, we expressed both the amounts of FRMs that we applied to the sample surface and those that we found within the lipid lamellae as the molar ratios of FRMs and lipids within the sample volume [further denoted as (FRM:L)_{applied} and (FRM:L)_{found}].

To calculate (FRM:L)_{applied} for the two SCS models, we employed the nominal amounts of FRMs and lipids used for sample preparation, and to calculate (FRM:L)_{found}—the amounts of FRMs and lipids found in the samples at the end of their preparation and rinsing. We dissolved the samples in 1 or 2 mL hexane:ethanol (2:1, v/v) and quantified the FRMs in the solution by GC/FID. In mixSCS samples, we quantified the FRM content immediately after performing FTIR or SAXD measurements. Since the FTIR measurements on topSCS samples took a long time, for experimental convenience we determined the FRM content not after the measurements but in samples prepared in parallel using the exact same procedures; to save the valuable perdeuterated FRMs, we prepared these samples using protonated FRMs. To estimate correctly the lipid amounts in the samples, we took into account the lipid losses resulting from the ethanol rinse. For untreated SCS and topSCS samples, we quantified the losses by comparing the integrated absorbances of the $\nu_s(\text{CH}_2)$ bands in spectra collected before and after rinsing. Depending on the FRM type and content, the average losses measured over the whole area of topSCS samples varied between 5.7 and 23.3% (the values

measured on individual spots of diameter 100–200 μm varied between 1 and 30%). For mixSCS samples, we estimated the lipid losses to be equal to those measured in untreated SCS samples, i.e., 17.4%.

To estimate (FRM:L)_{applied} and (FRM:L)_{found} for SC, we made two assumptions: (i) that the amounts of FRMs that have penetrated within the lipid lamellae can be approximated by those that were recovered with the 2nd to 30th stripping tapes (an assumption supported by the depth profiles of the FRM content within the SC, see Fig. S1 in Supplementary material); (ii) that the molar content of lipids in the volume of SC delimited by the application area of 0.95 cm^2 can be estimated assuming a uniform SC thickness of 15 μm and a lipid content within SC of 20% (w/w) [40]. We chose to use these assumptions instead of isolating the whole SC and quantifying its exact FRM content to avoid losses of the volatile FRMs during the heat separation of the SC. We used the lipid and FRM content of the SC layers reached by stripping with the first five tapes to estimate also the (FRM:L)_{found} in the upper SC layers.

2.6. FTIR

2.6.1. SC

We collected ATR-FTIR spectra from the SC sides of the skin samples (at least three different samples treated with each FRM) before and after stripping with 1, 3, 5, 10, 15, 20 and 30 tapes. To determine the depth within SC at which the spectra were collected we used the previously established procedure described in [40]. For more details, see Supplementary material.

2.6.2. MixSCS and topSCS

We collected transmission FTIR spectra from four to seven different spots of two or three samples for each composition. For mixSCS, the spots were circular with diameters of 100 or 200 μm , and for topSCS they were squares with dimensions of 170 \times 170 μm . We collected spectra from mixSCS immediately after preparation and rinsing, and from topSCS—6 or 16 h after the application of dFRM (to determine the effect of FRMs on the conformational order and the lateral packing of the lipid alkyl chains) and once again after rinsing the surface (to determine the mixing of FRMs with lipids). For more details, see Supplementary material.

2.6.3. Data treatment

We used the software OPUS 5.5 from Bruker (Germany). To determine the peak positions of the $\nu_s(\text{CH}_2)$ and $\nu_s(\text{CD}_2)$ bands we used a center of gravity algorithm applied at 95% of the peak height, after baseline-correcting the spectra between the endpoints of the $\nu_s(\text{CH}_2)$ and $\nu_s(\text{CD}_2)$ regions (for SC samples) or an algorithm based on the minima in second-derivative spectra (for SCS samples); the choice of these algorithms was based on the different shapes of the baselines and the different signal-to-noise ratios in spectra collected from the two substrates. To calculate the width of $\delta(\text{CH}_2)$ at 50% of the peak height in second-derivative spectra (denoted as FWHM_{scis}), we used the procedure described in detail in [17].

2.7. SAXD

We collected X-ray diffraction patterns from the mixSCS and topSCS samples (two samples for each composition) in a bench-top diffractometer D5000 from Siemens (Germany) for 1 or 2 h at room temperature. For topSCS, we collected diffraction patterns before and after the treatment of the same sample with FRMs. We collected also high-quality diffraction patterns from untreated SCS and topSCS containing CC using the beam line BM26B at the European Synchrotron Radiation Facility, ESRF (Grenoble, France). We collected diffraction patterns from two samples of each composition for 5 min at room temperature. For more details, see Supplementary material.

2.7.1. Data treatment

To compare diffraction patterns collected from the different samples we used one-dimensional plots of the scattering intensity I versus the scattering vector q calculated as $q = (4\pi\sin\theta)/\lambda$ (see Ref. [41] for the transformation of the two-dimensional synchrotron SAXD patterns into one-dimensional patterns). To facilitate the comparison, we baseline-corrected the bench-top diffraction patterns using the software OPUS 5.5 from Bruker (Germany) and a rubber-band function; subsequently, we normalized them to identical integrated areas of the sum of the 2nd and 3rd diffraction orders of the LPP, the 1st diffraction order of the SPP, and the 1st diffraction order of crystalline cholesterol, as these peaks were present in all samples. We calculated the repeat distance of the lamellar phases d from the positions of series of equidistant peaks (q_n) using $d = 2\pi/q_n$, where n is the order of the diffraction peak. We could use only the positions of the 2nd, 3rd and sometimes 4th diffraction orders of the LPP as the low signal-to-noise ratio precluded reliable detection of the higher orders. (Even though the partial overlap between the 2nd order of the LPP and the 1st order of the SPP made the determination of the peak position less accurate, we estimated that this uncertainty was not bigger than the one introduced by the broadness of the other diffraction peaks.) We calculated the electron density distribution within the LPP in untreated SCS and topSCS containing CC using the diffraction orders 1–6 of the LPP in diffraction patterns collected in the synchrotron as previously described [41,42].

3. Results and discussion

3.1. Content of FRMs in SC, mixSCS, and topSCS

To be a useful substitute for human skin in studies of the molecular interactions between topically applied chemicals and the SC lipids, a model system has to (i) incorporate these chemicals in quantities comparable to those that can be reached within the lipid matrix of human SC, and (ii) reflect faithfully their effects on the molecular organization of the SC lipids. Thus, we first compared the FRM content within the two SCS models with the one reached within SC following fairly heavy loading of the skin surface with FRMs (corresponding to application of approximately 3 μ moles of FRM per cm^2). The FRM doses that we used were many-fold higher than those found in real-life applications of fragrances, to facilitate the detection of the resulting effects and to estimate the upper limit of skin loading that can be reproduced in the two SCS models.

To enable this comparison despite the different lipid contents of SC and SCS, we expressed both the amounts of FRMs that we used in the sample preparation and those that we found within the lipid lamellae as the molar ratios of FRMs and lipids within the sample volume [further denoted as (FRM:L)_{applied} and (FRM:L)_{found}; see Materials and methods for details of the calculation].

Table 2 summarizes the experimental results obtained in the three systems. As expected, the FRM content within the SC gradually decreased from the surface to the inner layers (see also Fig. S1). Accordingly, the (FRM:L)_{found} estimated for the upper layers of SC (i.e., those removed by stripping with tapes 2 to 5) were higher than those averaged over

Table 2

FRM loading and content in SC, mixSCS, and topSCS. The amounts of FRMs are shown as the molar ratios of FRMs and lipids within the sample volumes. See text for details.

FRM	System	FRM:L _{applied} ^a	Application time [h]	FRM:L _{found} ^b
UL	SC	6.7	4	upper SC ^c : 0.93 ± 0.40
				whole SC ^d : 0.19 ± 0.06
	mixSCS	1.67	–	0.37 ± 0.06
			6	0.27 ± 0.08
DA	SC	7.27 \pm 0.42	16	0.52 ± 0.04
			4	upper SC ^c : 0.43 ± 0.31
	mixSCS	1.67	–	0.14 ± 0.05
			6	0.11 ± 0.02
CC	SC	5.33	16	0.97 ± 0.06
			4	upper SC ^c : 1.14 ± 0.51
	mixSCS	1.67	–	0.20 ± 0.02
			16	0.15 ± 0.02
		13.79 \pm 0.08	16	0.15 ± 0.02

^a Normalized amount of FRMs used for sample preparation.

^b Normalized amount of FRMs found in the samples.

^c Normalized amount of FRMs found in the SC layers removed by tapes 2 to 5.

^d Normalized amount of FRMs found in the SC layers removed by tapes 2 to 30.

the whole SC thickness, and the magnitude of the difference depended on the shape of the FRM gradient.

In mixSCS we reached (FRM:L)_{found} similar to those observed within the whole SC thickness; the (FRM:L)_{applied} that we were able to use, however, was three to four-fold lower than those we applied on skin. In samples prepared with (FRM:L)_{applied} ≥ 3.33 (i.e., a value almost two-fold lower than the one used on SC), we observed macroscopic liquid domains, indicating that the FRMs had phase-separated and could not be incorporated within the lipid lamellae during their self-assembly.

In topSCS we also obtained (FRM:L)_{found} similar to or higher than those observed within the whole SC thickness. We were able to modulate the UL and DA contents in the samples by varying the surface loading and the duration of the application period. Interestingly, we found identical relative amounts of CC in samples prepared using (CC:L)_{applied} ratios that differed by a factor of two.

In summary, the amounts of FRMs that we could incorporate within mixSCS and topSCS models were similar to those we found within the SC following fairly heavy loading of the skin surface. TopSCS, however, was able to support a broader range of (FRM:L)_{applied} than mixSCS.

3.2. Mixing of UL and DA with lipids in SC, mixSCS, and topSCS

FTIR spectroscopy of samples prepared with perdeuterated analogs of the FRMs allowed us to evaluate the degree of mixing between FRM and lipid molecules [43,44]. The position of the methylene symmetric stretching peak $\nu_s(\text{CH}_2)$ is diagnostic for the degree of conformational order in alkyl chains: it shifts to lower wavenumbers when the conformational order of the chains increases. Such relative ordering of the alkyl chains of UL and DA in respect to their conformation in solution is expected to occur if they mix with the structured lipids in the lamellae of SC and SCS. Since the $\nu_s(\text{CH}_2)$ band (originating from the lipids) and the $\nu_s(\text{CD}_2)$ band (originating from the FRMs) appear in different and well-separated spectral regions, we could analyze simultaneously the degree of conformational ordering of the deuterated alkyl chains of UL and DA and of the protonated alkyl chains of the lipids. The presence of only two methylene groups in the side chains of CC precluded such analysis of samples treated with this FRMs as the intensity of the $\nu_s(\text{CD}_2)$ band was too low to determine precisely its peak position.

Fig. 1 shows the shift in the positions of the $\nu_s(\text{CD}_2)$ peaks originating from dUL and dDA relative to their position in solution upon interaction of the FRMs with the lipids of SC, mixSCS, and topSCS. The $\nu_s(\text{CD}_2)$ bands of the two FRMs shifted to lower wavenumbers in all

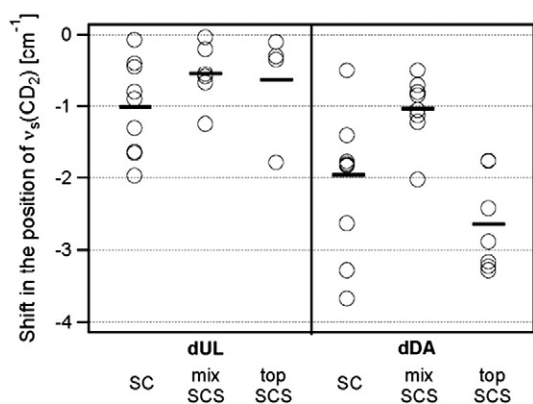


Fig. 1. Conformational ordering of the alkyl chains of UL and DA upon mixing with SC and SCS lipids. Shift of the position of $\nu_s(\text{CD}_2)$ bands originating from dUL (left panel) and dDA (right panel) in SC, mixSCS, and topSCS relative to their position in solution. For SC, the data points ($n = 10$) represent values measured at different depths within the SC in the course of tape-stripping of three to six different skin samples for each FRM. For mixSCS, the data points ($n = 6$ for dUL and $n = 8$ for dDA) represent values measured in samples containing (FRM:L)_{found} equal to 0.37 ± 0.06 and 0.14 ± 0.05 for dUL and dDA, respectively. For topSCS, the data points ($n = 4$ for dUL and $n = 7$ for dDA) represent values measured after rinsing the surface of two or three samples containing (FRM:L)_{found} equal to 0.27 ± 0.08 for dUL and 0.11 ± 0.02 for dDA. The bars represent the average values of the shift.

three supports, indicating that the alkyl chains of dUL and dDA mixed with the lipid molecules and thereby became more ordered than in solution. The shifts observed for dDA were larger than those observed for dUL in the same systems, indicating that the conformational disorder of the alkyl chains of UL was higher than the one of DA, most probably as a consequence of the bulkier head group and shorter length of the alkyl chains of UL compared to those of DA.

In summary, these results show that the alkyl chains of the FRMs incorporate in the lipid lamellae and mix with the lipid alkyl chains both in the SC and in the two synthetic models.

3.3. Effect of FRMs on the conformational order and the lateral packing of the lipid alkyl chains

To compare the effects that the FRMs exerted on the conformational ordering and the lateral packing of the lipid alkyl chains in SC and in the two synthetic models, we used two diagnostic spectroscopic parameters: the position of the $\nu_s(\text{CH}_2)$ peak as a measure for the average conformational ordering of the lipid chains, and the width of the methylene scissoring band $\delta(\text{CH}_2)$ (further denoted as $\text{FWHM}_{\text{scis}}$) as a measure for the relative content of OR lipid phases.

Fig. 2A and B shows representative examples of the depth variations of these two parameters observed in untreated SC and in SC treated with the three dFRM molecules. In qualitative agreement with previous reports [16,45,46], the position of the $\nu_s(\text{CH}_2)$ peak in untreated SC shifted to higher wavenumbers within the SC (from approximately 2847 cm^{-1} at the SC surface to 2851 cm^{-1} in the inner SC layers) indicating a gradual increase of the conformational disorder of the lipid chains (Fig. 2A). The incorporation of the dFRM within the SC led to a significant shift of the position of $\nu_s(\text{CH}_2)$ peak to higher wavenumbers in the topmost $1.5\text{--}2 \mu\text{m}$ of the SC indicating that the molecules induced conformational disorder of the SC lipid chains. The observed shift correlated well with the depth profiles of the FRM contents in the SC (see Fig. S1): it was highest at the SC surface and gradually decreased with the SC depth.

None of the three FRMs influenced significantly the depth profile of $\text{FWHM}_{\text{scis}}$ compared to the one observed in untreated SC (Fig. 2B). In both untreated and treated with FRM SC samples, the values of $\text{FWHM}_{\text{scis}}$ remained stable at around $11\text{--}12 \text{ cm}^{-1}$ throughout most of the

examined SC thickness, indicating that a large fraction of the SC lipids participated in OR lattices. The decrease of $\text{FWHM}_{\text{scis}}$ in the innermost SC layers, typical for native SC, was not influenced by the presence of FRMs. Apparently, neither the extent nor the depth distribution of OR phases within the SC was perturbed by the presence of FRMs.

Next, we investigated these spectroscopic parameters in the two synthetic models. In SCS samples prepared in the absence of FRMs, both the position of the $\nu_s(\text{CH}_2)$ peak ($2849.3 \pm 0.1 \text{ cm}^{-1}$) and the $\text{FWHM}_{\text{scis}}$ ($12.6 \pm 0.1 \text{ cm}^{-1}$) were close to those observed in untreated human SC and indicated that the alkyl chains in the SCS were conformationally ordered and packed predominantly in OR phases. (The difference of approximately 2 cm^{-1} in the positions of the $\nu_s(\text{CH}_2)$ peaks in SCS and in the surface layers of human SC reflects the well-known red-shifting of absorbance bands in spectra of bulk materials collected in ATR mode compared to their positions in transmission spectra [47].) The two spectroscopic parameters remained unchanged in mixSCS containing all three FRMs (Fig. 2C and D), indicating that the conformational order and lateral packing of the lipids had not changed upon inclusion of the FRMs in the lipid lamellae. This lack of effect is not surprising, considering that the FRM content in the mixSCS samples was more than two-fold lower than the one in the topmost $1.5\text{--}2 \mu\text{m}$ of the SC which caused conformational disorder of the lipids. Upon application of three-fold lower amounts of FRMs to the skin surface, the conformation and the lateral packing of the SC lipids also remained unchanged (data not shown); clearly, the effects of the chemicals on the lipid organization were dose-dependent.

Fig. 2E summarizes the changes that the incorporation of the FRMs caused to the position of the $\nu_s(\text{CH}_2)$ peak relative to those observed in the same spots of topSCS samples before application of the FRMs. These changes were qualitatively identical to the ones observed in SC. For all three FRMs we observed a shift of the position of $\nu_s(\text{CH}_2)$ towards higher wavenumbers indicating an increase of the conformational disorder of the lipid alkyl chains. For dUL and dDA, the magnitude of the shift increased with the FRM content of the layers. Not surprisingly, while having the same sign, the absolute magnitude of the shifts observed in topSCS was lower than those observed in SC. Since the FTIR spectra of topSCS were collected in transmission mode, they contained information averaged throughout the full thickness of the samples; thus, the magnitude of any spectral shifts that may have occurred in the FRM-rich topmost layers of the samples was lowered by signal originating from the inner layers of the topSCS samples which contained little if any FRMs. In contrast, by applying tape-stripping and ATR-FTIR spectroscopy to the skin samples we obtained spectroscopic information from thin layers of the SC, with thickness determined by the effective pathlength of the IR radiation in our setup (estimated from the Harrick's equation [47] to be equal to approximately $2.3 \mu\text{m}$ at 2850 cm^{-1} assuming a homogeneous incident angle of the IR beam equal to 45° and a refractive index of the SC equal to 1.5); thus, we could evidence the local perturbations that have occurred within the lipid lamellae of the topmost SC layers without averaging the spectroscopic information throughout the full SC thickness.

In topSCS samples with (FRM:L)_{found} similar to those in SC, we observed the same lack of effect of the FRMs on $\text{FWHM}_{\text{scis}}$ as in SC (Fig. 2F). The values of $\text{FWHM}_{\text{scis}}$ remained identical to those in untreated SCS and dropped by an average of 1.75 cm^{-1} only for dDA when its average content in the layers reached (FRM:L)_{found} = 0.97 ± 0.06 , a value two-fold higher than the dDA content within the topmost SC layers in which it had no effect on $\text{FWHM}_{\text{scis}}$. As discussed above, the values of (FRM:L)_{found} reflect the average content of the FRMs throughout the topSCS thickness; thus, it is highly probable that the differences of the lateral lipid packing observed in the two systems were due to the many-fold higher local content of dDA in the upper layers of topSCS compared to the one in the topmost SC layers.

In summary, both mixSCS and topSCS reproduced qualitatively the existence and the dose-dependence of the effects that the FRMs caused on the conformational order and lateral packing of the lipids in SC.

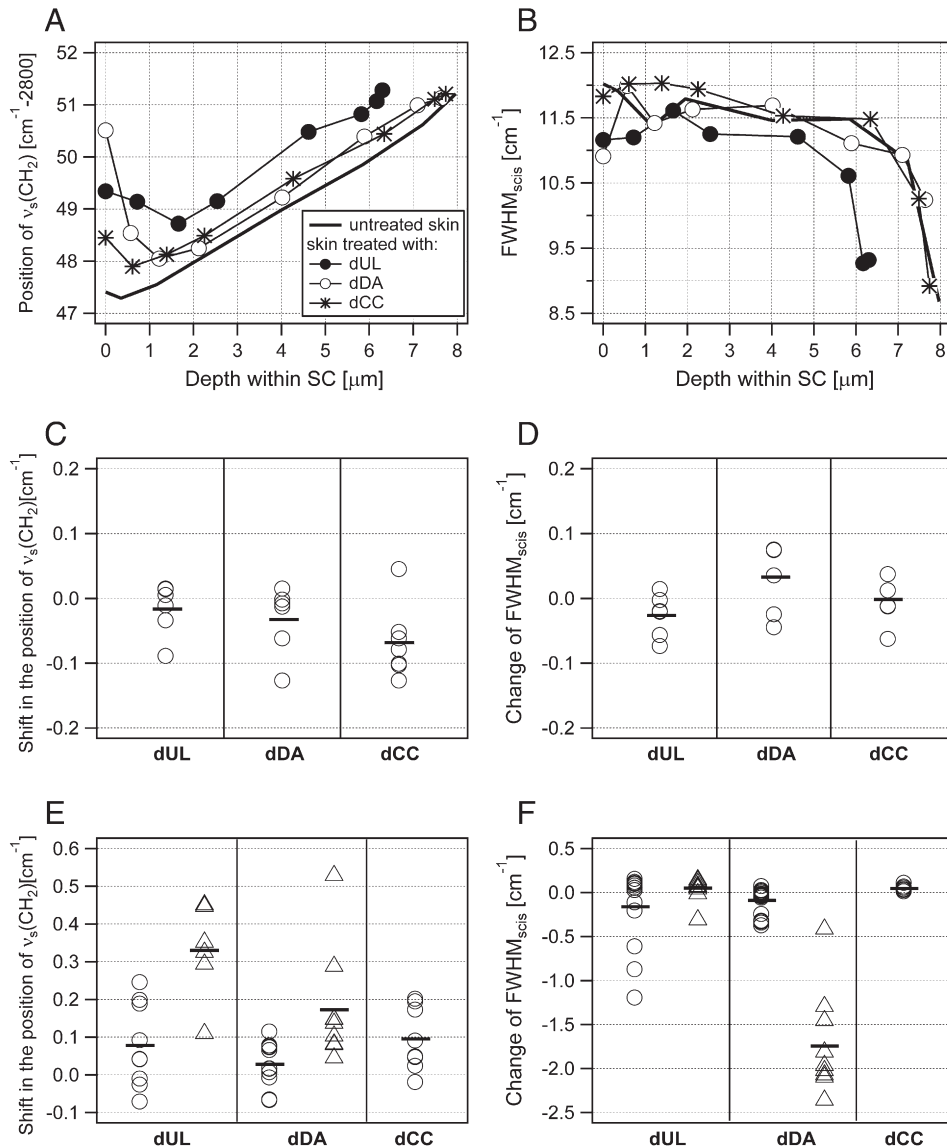


Fig. 2. Influence of FRMs on the conformational order and the lateral organization of the lipids in human SC (A, B), mixSCS (C, D), and topSCS (E, F). (A, B) Typical depth profiles of the position of the $\nu_s(\text{CH}_2)$ peak (A) and the $\text{FWHM}_{\text{scis}}$ (B) in spectra collected from untreated SC and following application of dFRM. The symbols represent the values of the two parameters in spectra collected in the course of tape-stripping of the SC; the connecting lines are for guidance of the eye only. Data from skin of one donor. The values of $(\text{FRM:L})_{\text{found}}$ within the upper SC layers (*i.e.*, those removed by the first five tapes) were equal to 0.93 ± 0.40 , 0.43 ± 0.31 , and 1.14 ± 0.51 for dUL, dDA, and dCC, respectively. (C–F) Shift in the position of the $\nu_s(\text{CH}_2)$ peak (C, E) and change of $\text{FWHM}_{\text{scis}}$ (D, F) in spectra collected from mixSCS (C, D) and topSCS (E, F) relative to those in spectra collected from untreated SCS. In the mixSCS samples, the values of $(\text{FRM:L})_{\text{found}}$ were equal to 0.37 ± 0.06 , 0.14 ± 0.05 , and 0.20 ± 0.02 for dUL, dDA, and dCC, respectively. In the topSCS samples, the values of $(\text{FRM:L})_{\text{found}}$ for dUL were equal to 0.27 ± 0.08 and 0.52 ± 0.04 (shown respectively as circles and triangles), for dDA were equal to 0.11 ± 0.02 and 0.97 ± 0.06 (shown respectively as circles and triangles), and for dCC were equal to 0.15 ± 0.02 . Each data point corresponds to the value observed in a spectrum collected from one spot of the sample. The bars represent the average value of the shift.

3.4. Effect of FRMs on the lamellar lipid organization

In addition to the effects of the FRMs on the lateral lipid organization, using SAXD of mixSCS and topSCS we could also assess how the FRMs influence three important parameters of the lamellar lipid organization: the presence of LPP and SPP, the repeat distance of the LPP, and the density distribution within the unit cell of the LPP. Fig. 3 shows typical diffraction patterns collected from untreated SCS, mixSCS and topSCS using a bench-top diffractometer. In agreement with earlier reports [11,27], the patterns of untreated SCS displayed peaks associated with the LPP (located at approximately 1.1, 1.6, and 2.1 nm^{-1}), SPP (located at approximately 1.2 and 2.4 nm^{-1}), and crystalline cholesterol (located at approximately 1.9 nm^{-1}); the corresponding repeat distances calculated for the LPP and SPP were equal to 11.8 nm (Fig. 4A) and 5.3 nm , respectively. In the patterns collected from mixSCS (Fig. 3A),

the positions of the peaks associated with the LPP were shifted to lower q -values, indicating the swelling of this phase; the repeat distances calculated for LPP in mixSCS containing UL, DA, and CC were 4, 3, and 2% higher than those observed in untreated SCS (Fig. 4B). The position and the corresponding repeat distance of the SPP in these layers remained unchanged. The presence of the FRMs during the self-assembly of the lipid lamellae affected to a different extent the relative content of the two lipid phases, as estimated from the relative contributions of the peaks associated with the two phases to the normalized patterns shown in Fig. 3A: while in mixSCS containing UL the ratio of LPP/SPP was similar to the one observed in untreated SCS, in mixSCS containing DA and CC it was noticeably higher than in untreated SCS.

The diffraction patterns collected from topSCS also contained peaks associated with LPP, SPP, and crystalline cholesterol (Fig. 3B). The

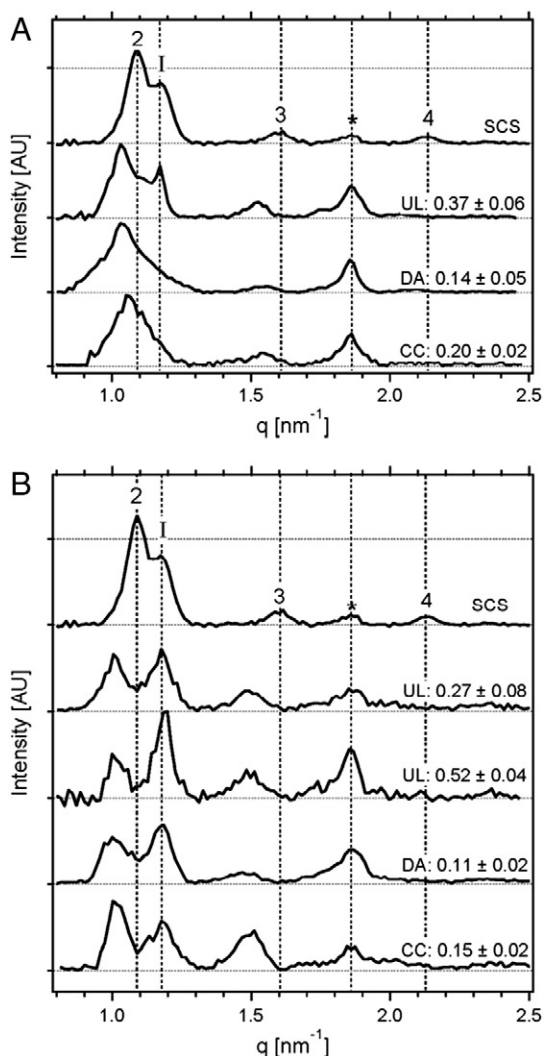


Fig. 3. Lamellar organization in untreated, mixSCS, and topSCS. Typical diffraction patterns collected from untreated SCS and mixSCS (A) and untreated SCS and topSCS (B). The numbers on top of the patterns indicate the (FRM:L)_{found} in the samples. Arabic (2 to 4) and Roman (I) numbers mark the orders of the diffraction peaks of LPP and SPP, respectively, and an asterisk – the 1st order of diffraction of crystalline cholesterol. The vertical dotted lines indicate these peak positions in samples of untreated SCS.

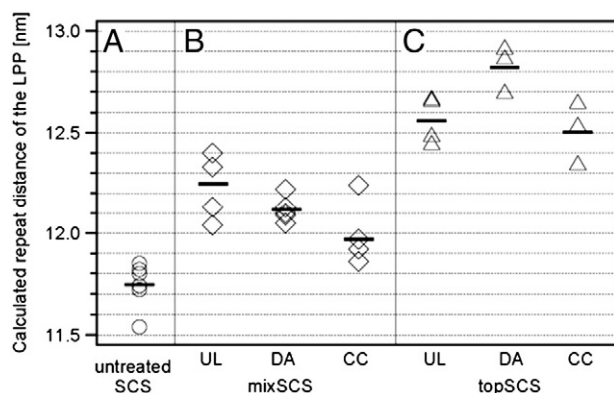


Fig. 4. Repeat distance of the LPP calculated for untreated SCS (A), mixSCS with (FRM:L)_{found} equal to 0.37 ± 0.06 , 0.14 ± 0.05 , and 0.20 ± 0.02 for UL, DA, and CC, respectively (B), and topSCS with (FRM:L)_{found} equal to 0.27 ± 0.08 , 0.11 ± 0.02 , and 0.15 ± 0.02 for UL, DA, and CC, respectively (C). Each data point represents a repeat distance calculated from one of the diffraction orders of the LPP in patterns collected from two different samples for each composition. The bars show the average repeat distance calculated for each SCS.

positions of the peaks attributed to the 2nd and 3rd diffraction orders of the LPP were shifted to even lower q -values than those in mixSCS, indicating that the topical application of FRMs increased the repeat distance of the LPP even further. The repeat distances calculated for topSCS containing UL, DA, and CC were 7, 9, and 6% higher than those calculated for untreated SCS (Fig. 4C); for UL, this swelling of the LPP was independent of the FRM content in the layers, as evidenced by the identical positions of the peaks associated with the LPP in patterns collected from samples of different (FRM:L)_{found} values. Similarly to mixSCS, the position of the peaks associated with the SPP remained unchanged compared to those observed in untreated SCS. In the patterns collected from topSCS treated with UL and DA we observed a dose-dependent decrease of the content of lamellar phases: the overall signal-to-noise ratio in the normalized patterns of topSCS treated with UL decreased considerably with increasing the FRM content in the lamellae (Fig. 3B), and samples of topSCS containing relatively high amounts of DA [(FRM:L)_{found} = 0.97 ± 0.06] produced no measurable patterns (data not shown).

The swelling of the LPP observed in both mixSCS and topSCS, the unchanged repeat distance of the SPP, and the dose-dependence of the content of LPP indicate that the FRMs interacted predominantly with (and inserted into) the LPP and only a little (if at all) with the SPP. The data in Figs. 3 and 4, however, give no indication if the distribution of the FRMs within the unit cell of the LPP was homogeneous or if the FRM molecules were located at a particular portion of the unit cell. Because of the high contrast that perdeuterated molecules give in the diffraction pattern, neutron diffraction studies would be, in principle, ideally suited to address this question [48]. Unfortunately, the density profile of the scattering length in LPP is not known; in our experience, obtaining it is not a trivial task. Since water molecules are present not only at the borders but also within the unit cell of the LPP, the identification of the phase signs is not straightforward and goes well beyond the scope of the present work. SAXD analysis however, provides a useful alternative to calculate the distribution of the FRM molecules since the electron density profile of the LPP has been previously established [42]. The distribution of the FRM molecules can be obtained by calculating the electron density distribution within the unit cell of LPP using high-resolution diffraction patterns (*i.e.*, ones with considerably higher signal-to-noise ratio than the patterns collected using a bench-top diffractometer shown in Fig. 3) and an appropriately chosen set of phase signs [14,42,49]. As a demonstration of principle, we probed the position of CC from the distribution of the electron density of the LPP in patterns collected using a synchrotron from untreated SCS and topSCS (see Fig. S2), as the swelling of the LPP in this model was considerably higher than the one observed in mixSCS. We used the set of phase signs ($- + - + - +$) that we determined earlier from structure factor amplitudes calculated for untreated SCS of eight different compositions [42]. The structure factor amplitudes calculated with this set of phase signs for untreated SCS and topSCS containing CC fit well to the Fourier curve associated with LPP that we determined in [42]; the high quality of the fit (R^2 values of 0.916 and 0.951) validated our choice of the phase solution.

Fig. 5 compares the electron density distribution within the LPP in untreated SCS and topSCS containing CC. Both curves displayed four main regions of high electron density positioned around ± 6 and ± 2 nm from the center of the unit cell. Earlier, we have ascribed these peaks to the location of ceramide headgroups within the trilayer structure in the unit cell of the LPP [14,42]. While the overall pattern of the density distribution in topSCS was similar to the one in untreated SCS, the positions of the high density regions observed in the two samples, however, differed significantly: the spacing between the peaks of high density was equal to 4.5, 2.8 and 4.5 nm in untreated SCS (resulting in a unit cell of 11.8 nm) and to 4.5, 3.8, and 4.5 nm in topSCS (resulting in a unit cell of 12.8 nm). Apparently, the swelling of the LPP caused by incorporation of CC in topSCS was limited only to the central region of the LPP, thus suggesting (predominant) localization of CC within this

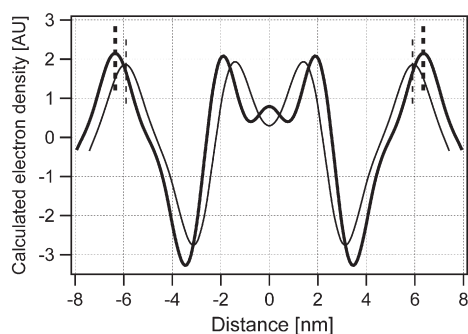


Fig. 5. Distribution of the electron density around the center of the unit cell of LPP (positioned at 0 nm) in untreated SCS (thin line) and topSCS containing CC with (FRM:L)_{found} equal to 0.15 ± 0.02 (thick line). The thin and thick dashed lines indicate the boundaries of the unit cells in untreated SCS and in topSCS containing CC, respectively.

region. Such localization fits well with the sandwich model for the organization of LPP which postulates a central region containing relatively disordered alkyl chains sandwiched between two peripheral regions containing crystalline alkyl chains [11]. Thus, it is not surprising to find the CC molecules accommodated within the less dense central region without interfering with the OR-packed lipids in the peripheral regions; our data on the unchanged OR packing upon insertion of CC (see Fig. 2) further support this hypothesis.

4. Conclusions

In this work, we investigated the possibility to reproduce the interactions between volatile organic chemicals and the SC barrier lipids in two synthetic lipid models. Our results show that it is possible to incorporate these chemicals within the lipid lamellae of the models in quantities comparable to those reached within the SC of excised human skin. Both the existence and the dose-dependence of the effects that these molecules exerted on the lateral organization of the SC lipids could be qualitatively reproduced in the SCS. The SCS models also facilitated the investigation of the lamellar organization of the barrier lipids by SAXD which is considerably more difficult using SC isolated from excised skin [50,51]; thus, we could elucidate the nature of the interaction between the chemicals and the lipid lamellae (disruption or non-perturbing insertion) and the position of the exogenous molecules within the unit cell of the LPP.

When comparing the suitability of the two SCS models to study the effects of topically applied chemicals, topSCS emerged as more appropriate than mixSCS. In it, the chemicals were applied on top of preformed lipid lamellae of appropriate 3D structure, and—contrary to the situation in mixSCS—did not interfere with the self-assembly of the lipids. Furthermore, the FRM distribution within topSCS was most probably inhomogeneous with a content gradually decreasing with depth, similar to the gradients observed in SC and unlike the expected homogeneous FRM distribution within mixSCS. Finally, topSCS was able to support a broader range of (FRM:L)_{applied} than mixSCS and can, therefore, be used in more extensive dose–response studies. Nonetheless, it is important to keep in mind that the structure of topSCS is considerably more labile than the one of native SC in which the stability of the lipid lamellae is greatly enhanced by the presence of corneocytes.

One practical limitation that the SCS models imposed on the studies of skin–fragrance interactions is that they did not allow determination of the depth profiles of FRM contents and lateral lipid organization which we could achieve in SC by combining tape-stripping with GC and ATR–FTIR. Regarding the molecular organization of the lipid lamellae, however, it should be possible to collect spectra from increasingly thicker layers of the SCS lamellae using ATR–FTIR spectroscopy with variable angle of incidence [52], and thus follow the

relative changes of different spectroscopic parameters within the SCS thickness. The SCS models have one important advantage over SC in spectroscopic studies: they offer the possibility to investigate the hydrogen bonding between the head groups of the barrier lipids following the spectroscopic changes in the amide regions, which is not possible using SC as these regions are dominated by the keratin absorption [26,53]. We will explore these two options in our future studies.

The model systems developed in this work offer a useful *in vitro* alternative to excised skin to study the effects of topically applied chemicals on the SC lipids, and thus contribute to the ongoing push to shift the safety testing of chemicals to *in vitro* studies [54–56]. Importantly, they offer the possibility to mimic the modified lamellar structure and organization of diseased SC by subtle changes of the lipid composition; thus, they are well suited to investigate the different impact that chemicals can have on healthy and diseased skin. The use of such synthetic SC replacements is certainly not limited to testing the action of fragrance materials on the lipids of the skin barrier. The systems we present here can easily be extended to many other classes of chemicals which may come in contact with the SC lipids, and which can adversely modify the skin barrier properties. Thus, they can find broad application in the areas of product safety, healthcare, drug delivery, and national security.

Acknowledgements

We thank Dr Edmond Koller, the group of DPMC at the University of Geneva, and the personnel at the DUBBLE beam line at the ESRF for assistance with the SAXD measurements, and the Dutch Organization for Scientific Research (NWO) for providing beam time at the ESRF.

Appendix A. Supplementary data

Supplementary data to this article can be found online at <http://dx.doi.org/10.1016/j.bbamm.2013.10.006>.

References

- [1] P.M. Elias, Stratum corneum defensive functions: an integrated view, *J. Invest. Dermatol.* 125 (2005) 183–200.
- [2] C.R. Harding, The stratum corneum: structure and function in health and disease, *Dermatol. Ther.* 17 (2004) 6–15.
- [3] J.A. Bouwstra, M. Poncet, The skin barrier in healthy and diseased state, *Biochim. Biophys. Acta Biomembr.* 1758 (2006) 2080–2095.
- [4] M. Boncheva, Molecular organization of the lipid matrix in stratum corneum and its relevance for the protective functions of human skin, in: M. Loden, H.I. Maibach (Eds.), *Treatment of Dry Skin Syndrome*, Springer-Verlag, Berlin, 2012, pp. 125–147.
- [5] K.R. Feingold, The role of epidermal lipids in cutaneous permeability barrier homeostasis, *J. Lipid Res.* 48 (2007) 2531–2546.
- [6] K.C. Madison, Barrier function of the skin: “la raison d’être” of the epidermis, *J. Invest. Dermatol.* 121 (2003) 231–241.
- [7] R.O. Potts, M.L. Francoeur, Lipid biophysics of water loss through the skin, *Proc. Natl. Acad. Sci. U. S. A.* 87 (1990) 3871–3873.
- [8] P.W. Wertz, B. van der Bergh, The physical, chemical, and functional properties of lipids in the skin and other biological barriers, *Chem. Phys. Lipids* 91 (1998) 85–96.
- [9] C.R. Harding, D.J. Moore, A.V. Rawlings, Ceramides and the skin, in: R. Baran, H.I. Maibach (Eds.), *Textbook of Cosmetic Dermatology*, Informa Healthcare, New York, 2010, pp. 150–164.
- [10] L. Norlén, I. Nicander, A. Lundsjö, T. Cronholm, B. Forslind, A new HPLC-based method for the quantitative analysis of inner stratum corneum lipids with special reference to the free fatty acid fraction, *Arch. Dermatol. Res.* 290 (1998) 508–516.
- [11] J.A. Bouwstra, Lipid organization of the skin barrier, in: A.V. Rawlings, J.J. Leyden (Eds.), *Skin Moisturization*, Informa Healthcare USA Inc., New York, 2009, pp. 17–40.
- [12] D.C. Swartzendruber, P.W. Wertz, D.J. Kitko, K.C. Madison, D.T. Downing, Molecular models of the intercellular lipid lamellae in mammalian stratum corneum, *J. Invest. Dermatol.* 92 (1989) 251–257.
- [13] J.R. Hill, P.W. Wertz, Molecular models of the intercellular lamellae from epidermal stratum corneum, *Biochim. Biophys. Acta* 1616 (2003) 121–126.
- [14] T.J. McIntosh, Organization of skin stratum corneum extracellular lipid lamellae: diffraction evidence for asymmetric distribution of cholesterol, *Biophys. J.* 85 (2003) 1675–1681.
- [15] J.A. Bouwstra, G.S. Gooris, M. Poncet, The lipid organization of the skin barrier: liquid and crystalline domains coexist in lamellar phases, *J. Biol. Phys.* 28 (2002) 211–223.

- [16] R. Mendelsohn, C.R. Flach, D.J. Moore, Determination of molecular conformation and permeation in skin via IR spectroscopy, microscopy, and imaging, *Biochim. Biophys. Acta* 1758 (2006) 923–933.
- [17] M. Boncheva, F. Damien, V. Normand, Molecular organization of the lipid matrix in intact stratum corneum using ATR–FTIR spectroscopy, *Biochim. Biophys. Acta Biomembr.* 1778 (2008) 1344–1355.
- [18] K. Babita, V. Kumar, V. Rana, S. Jain, A.K. Tiwary, Thermotropic and spectroscopic behavior of skin: relationship with percutaneous permeation enhancement, *Curr. Drug Deliv.* 3 (2006) 95–113.
- [19] M. de Jager, W. Groenink, R.B.I. Guivernau, E. Andersson, N. Angelova, M. Poncet, J.A. Bouwstra, A novel in vitro percutaneous penetration model: evaluation of barrier properties with p-aminobenzoic acid and two of its derivatives, *Pharm. Res.* 23 (2006) 951–960.
- [20] F. Damien, M. Boncheva, The extent of orthorhombic lipid phases in the stratum corneum determines the barrier efficiency of human skin in vivo, *J. Invest. Dermatol.* 130 (2010) 611–614.
- [21] D. Groen, D. Poole, G.S. Gooris, J.A. Bouwstra, Is an orthorhombic lateral packing and a proper lamellar organization important for the skin barrier function? *Biochim. Biophys. Acta* 1808 (2011) 1529–1537.
- [22] F. Berthaud, M. Boncheva, Correlation between the properties of the lipid matrix and the degrees of integrity and cohesion in healthy human stratum corneum, *Exp. Dermatol.* 20 (2011) 255–262.
- [23] V.M. Meidan, C.S. Roper, Inter- and intra-individual variability in human skin barrier function: a large scale retrospective study, *Toxicol. In Vitro* 22 (2008) 1062–1069.
- [24] L. Norlén, I. Nicander, B.L. Rozell, S. Ollmar, B. Forslind, Inter- and intra-individual differences in human stratum corneum lipid content related to physical parameters of skin barrier function in vivo, *J. Invest. Dermatol.* 112 (1999) 72–77.
- [25] J. Caussin, G.S. Gooris, M. Janssens, J.A. Bouwstra, Lipid organization in human and porcine stratum corneum differs widely, while lipid mixtures with porcine ceramides model human stratum corneum lipid organization very closely, *Biochim. Biophys. Acta* 1778 (2008) 1472–1482.
- [26] M.E. Rerek, D.J. Moore, Skin lipid structure: insight into hydrophobic and hydrophilic driving forces for self-assembly using IR spectroscopy, in: L.D. Rhein, M. Schlossman, A. O'Lenick, P. Somasundran (Eds.), *Surfactants in Personal Care Products and Decorative Cosmetics*, CRC Press, Boca Raton, 2007, pp. 189–209.
- [27] J.A. Bouwstra, G.S. Gooris, The lipid organization in human stratum corneum and model systems, *Open Dermatol. J.* 4 (2010) 10–13.
- [28] J.A. Bouwstra, G.S. Gooris, F.E.R. Dubbelaar, M. Poncet, Phase behavior of stratum corneum lipid mixtures based on human ceramides: the role of natural and synthetic ceramide 1, *J. Invest. Dermatol.* 118 (2002) 606–617.
- [29] D. Groen, G.S. Gooris, M. Poncet, J.A. Bouwstra, Two new methods for preparing a unique stratum corneum substitute, *Biochim. Biophys. Acta* 1778 (2008) 2421–2429.
- [30] M. de Jager, W. Groenink, J. van der Spek, C. Janmaat, G.S. Gooris, M. Poncet, J.A. Bouwstra, Preparation and characterization of a stratum corneum substitute for in vitro percutaneous penetration studies, *Biochim. Biophys. Acta Biomembr.* 1758 (2006) 636–644.
- [31] D. Groen, D.S. Poole, G.S. Gooris, J.A. Bouwstra, Investigating the barrier function of skin lipid models with varying compositions, *Eur. J. Pharm. Biopharm.* 79 (2011) 334–342.
- [32] J. Caussin, G.S. Gooris, W. Groenink, J.W. Wiechers, J.A. Bouwstra, Interaction of lipophilic moisturizers on stratum corneum domains in vitro and in vivo, *Skin Pharmacol. Physiol.* 20 (2007) 175–186.
- [33] J.W. Wiechers, J.C. Dederen, A.V. Rawlings, Moisturization mechanisms: internal occlusion by orthorhombic lipid phase stabilizers—a novel mechanism of action of skin moisturization, in: A.V. Rawlings, J.J. Leyden (Eds.), *Skin Moisturization*, Informa Healthcare USA, Inc., New York, 2009, pp. 309–321.
- [34] P.W. Wertz, D.T. Downing, Epidermal lipids, in: L.A. Goldsmith (Ed.), *Physiology, Biochemistry, and Molecular Biology of the Skin*, Oxford University Press, 1991, pp. 205–236.
- [35] M. de Jager, G.S. Gooris, M. Poncet, J.A. Bouwstra, Lipid mixtures prepared with well-defined synthetic ceramides closely mimic the unique stratum corneum lipid phase behaviour, *J. Lipid Res.* 46 (2005) 2649–2656.
- [36] J. van Smeden, L. Hoppel, R. van der Heijden, T. Hankemeier, R.J. Vreeken, J.A. Bouwstra, LC/MS analysis of stratum corneum lipids: ceramide profiling and discovery, *J. Lipid Res.* 52 (2011) 1211–1221.
- [37] M. Janssens, G.S. Gooris, J.A. Bouwstra, Infrared spectroscopy studies of mixtures prepared with synthetic ceramides varying in head group architecture: coexistence of liquid and crystalline phases, *Biochim. Biophys. Acta* 1788 (2009) 732–742.
- [38] F. Berthaud, S. Narancic, M. Boncheva, In vitro skin penetration of fragrances: trapping the evaporated material can enhance the dermal absorption of volatile chemicals, *Toxicol. In Vitro* 25 (2011) 1399–1405.
- [39] Organization for Economic Cooperation and Development, OECD, Test no. 428: skin absorption: in vitro method, OECD Guidelines for the Testing of Chemicals, 12009. 1–8.
- [40] M. Boncheva, J. de Sterke, P.J. Caspers, G.J. Puppels, Depth profiling of stratum corneum hydration in vivo: a comparison between conductance and confocal Raman spectroscopic measurements, *Exp. Dermatol.* 18 (2009) 870–876.
- [41] J.F. Nagle, S. Tristram-Nagle, Structure of lipid bilayers, *Biochim. Biophys. Acta* 1469 (2000) 159–195.
- [42] D. Groen, G.S. Gooris, J.A. Bouwstra, New insights into the stratum corneum lipid organization by X-ray diffraction analysis, *Biophys. J.* 97 (2009) 2242–2249.
- [43] R. Mendelsohn, M.E. Rerek, D.J. Moore, Infrared spectroscopy and microscopic imaging of stratum corneum models and skin, *Phys. Chem. Chem. Phys.* 2 (2000) 4651–4657.
- [44] R.G. Snyder, M.C. Goh, V.J.P. Srivatsavoy, H.L. Strauss, D.L. Dorset, Measurement of the growth kinetics of microdomains in binary n-alkane solid solutions by infrared spectroscopy, *J. Phys. Chem.* 96 (1992) 10008–10019.
- [45] F. Damien, M. Boncheva, Influence of cosmetic formulations on the molecular organization of stratum corneum lipids and the barrier efficiency of human skin in vivo, *J. Pharm. Pharmacol.* 62 (2010) 794.
- [46] P. Dumas, L. Miller, The use of synchrotron infrared microspectroscopy in biological and biomedical investigations, *Vib. Spectrosc.* 32 (2003) 3–21.
- [47] N.J. Harrick, *Internal Reflection Spectroscopy*, Harrick Scientific Corporation, NY, 1987.
- [48] D.L. Worcester, N.P. Franks, Structural analysis of hydrated egg lecithin and cholesterol bilayers, *J. Mol. Biol.* 100 (1976) 359–378.
- [49] S.H. White, D. Mirejovsky, G.J. King, Structure of lamellar lipid domains and corneocyte envelopes of murine stratum corneum: an X-ray diffraction study, *Biochemistry* 27 (1988) 3725–3732.
- [50] J.A. Bouwstra, G.S. Gooris, J. van der Spek, W. Bras, Structural investigations of human stratum corneum by small-angle X-ray scattering, *J. Invest. Dermatol.* 97 (1991) 1005–1012.
- [51] V. Schreiner, G.S. Gooris, S. Pfeiffer, G. Lanzendoerfer, H. Wenck, W. Diembeck, E. Proksch, J.A. Bouwstra, Barrier characteristics of different human skin types investigated with X-ray diffraction, lipid analysis, and electron microscopy imaging, *J. Invest. Dermatol.* 114 (2000) 654–660.
- [52] K.L.A. Chan, S.G. Kazarian, ATR FTIR imaging with variable angle of incidence: a three-dimensional profiling of heterogeneous materials, *Appl. Spectrosc.* 61 (2007) 48–54.
- [53] D.J. Moore, M.E. Rerek, Insight into the molecular organization of lipids in the skin barrier from infrared spectroscopy studies of stratum corneum lipid models, *Acta Derm. Venereol. Suppl.* 208 (2000) 16–22.
- [54] Scientific Committee on Consumer Safety, SCCS, Basic Criteria for the In Vitro Assessment of Dermal Absorption of Cosmetic Ingredients, 2010. (Web 31 July, 2013, http://ec.europa.eu/health/scientific_committees/consumer_safety/docs/sccs_s_002.pdf).
- [55] R. Combes, M. Barratt, M. Balls, An overall strategy for the testing of chemicals for human hazard and risk assessment under the EU REACH system, *Altern. Lab. Anim. (ALTA)* 31 (2003) 7–19.
- [56] A.P. Worth, M. Balls, The principles of validation and the ECVAM validation process, *ATLA* 30 (2002) 15–21.